Available online at www.sciencedirect.com
ScienceDirect
Trans. Nonferrous Met. Soc. China 34(2024) 935−951
Transactions of Nonferrous Metals Society of China
www.tnmsc.cn

Effect of extrusion speed on properties of Cu−5vol.%Ti_2SnC composite wire fabricated by friction stir back extrusion process

Amirhossein JAHANI, Hamed JAMSHIDI AVAL, Mohammad RAJABI, Roohollah JAMAATI

Department of Materials Engineering, Babol Noshirvani University of Technology, Shariati Avenue, Babol 47148-71167, Iran

Received 24 September 2022; accepted 11 May 2023

Abstract: The effect of axial traverse speed of friction stir back extrusion (FSBE) process on the microstructure, mechanical, electrical, and wear properties of Cu−Ti_2SnC composite wire was investigated. The FSBE process was performed on the primary composite made by the powder metallurgy method with 5 vol.% of Ti_2SnC MAX phase. The results showed that as the extrusion speed increased, the twins formed in the microstructure increased, the Ti_2SnC particles became finer, and the interface of bonding of the MAX phase−Cu matrix improved. The Cu−Ti_2SnC composite wire fabricated at the rotational speed of 600 r/min and axial traverse speed of 25 mm/min showed the maximum hardness, yield strength, and ultimate tensile strength of HV 132.7, 278.34 MPa, and 485.15 MPa, respectively. This finding was due to its strong interfacial bonding and fine MAX phase particles. Besides, the larger grain size, the better interface bonding, and the lower the porosity resulted in the highest electrical conductivity of 89.21% (IACS) and least wear rate of 0.0015 mg/m of Cu−Ti_2SnC composite wire fabricated at rotational speed of 600 r/min and axial traverse speed of 25 mm/min.

Key words: friction stir back extrusion; Ti_2SnC MAX phase; copper matrix composite; electrical conductivity

1 Introduction

Copper is broadly used in electrical applications because of its excellent electrical conductivity but has poor mechanical strength. Therefore, it should be strengthened by, for example, making copper matrix composites (CMCs) to have electrical conductivity and strength [1−5]. Using ceramic particles to achieve high strength, hardness, and wear resistance is also a proper choice [6,7], but this type of CMC fabrication usually results in low electrical conductivity [8−11].

However, the $M_{n+1}AX_n$ phase (MAX) has good electrical and thermal conductivity, machinability, high elastic moduli, and corrosion resistance. In this phase, M is an early transition metal, A is an element in the periodic table from columns 13 to 16, and X is carbon or nitrogen. Among the MAX phases, the Ti_2SnC, with good mechanical properties, has the lowest electrical resistivity (0.22 μΩ·m) [12]. Considering the properties of MAX phases (especially Ti_2SnC), it is a proper choice to fabricate CMCs.

A few limited sources have reported the fabrication of CMCs reinforced by MAX phase [13]. For instance, WU et al [10,14−16] created a Cu−Ti_2SnC composite by hot pressing. They then studied the microstructure and mechanical properties of the composite. They mixed copper powder and Ti_2SnC under an argon gas atmosphere at different time to make a Cu−Ti_2SnC composite. Afterward, the material was subjected to a hot press at 859, 950 and 1050 °C for 0.5 h. The results showed that adding the MAX phase reduced the grain size significantly and wear rate, and adding

Corresponding author: Hamed JAMSHIDI AVAL, Tel: +98-11-35501808, Fax: +98-11-35501800, E-mail: h.jamshidi@nit.ac.ir
DOI: 10.1016/S1003-6326(23)66444-1

5 vol.% of MAX phase increased the yield strength to 188 MPa. They also reported that although the formation of a reactive layer at the copper−MAX phase interface improved the mechanical properties, it weakened the electrical conductivity.

Generally, CMCs are fabricated using two methods: liquid state and solid state [8]. The main problems are the liquid state methods' wettability, formation reaction layer, and porosity [2]. Moreover, friction stir back extrusion (FSBE), a new thermo-mechanical technique based on friction stir processing, is proper for fabricating composite material. This process has been recently used for fine-grained wires and tube fabrication. In addition, LI et al [17] have recently studied the fabrication of copper−carbon composite wire using the FSBE method. They reported that ten-fold reductions of both copper grain size and carbon particle size were achieved and the carbon powder was refined to a sub-micron level and uniformly dispersed in the copper matrix. Furthermore, the composite wire had 30% higher heat capacity and 29% lower density than the sample without reinforcement.

According to the authors' knowledge in the present study, the effect of extrusion speed in fabrication Cu−5vol.%Ti_2SnC composite using the FSBE process was not studied previously. In this study, the FSBE method created CMCs wires with 5 vol.% Ti_2SnC due to the FSBE process capabilities and the Ti_2SnC MAX phase unique characteristics. Besides, prefabricated Cu−5vol.% Ti_2SnC composites formed by the powder metallurgy method were employed to fabricate composite wire. Moreover, the FSBE axial traverse speed effects on microstructure and mechanical, tribological, and electrical properties of composite wires were investigated.

2 Experimental

In the current study, electrolytic copper powder with an average particle size of 5 μm and Ti_2SnC powder as reinforcement with an average particle size of 15 μm were used. Figure 1 shows the scanning electron microscope (SEM) images of Ti_2SnC and copper powders. For fabricating Cu−Ti_2SnC composite, a mixture of copper and Ti_2SnC powders with a constant volume fraction of 5% of MAX phase was prepared. Then, under the protection of Ar gas, the mixed powder was ball milled for 10 min with a rotation speed of 300 r/min using a planetary ball mill (model: PM) with a ball-to-material ratio of 5:1. In addition, for cylindrical primary composite fabrication with 20 mm in diameter and 30 mm in length, the mixed powder was poured into the cold pressing die. It was cold pressed under a pressure of 15 MPa. After this stage, the primary composite was placed into the Ar gas protective atmosphere furnace at 850 °C for 30 min. Finally, the FSBE process was executed on sintered composites. FSBE was carried out using a punch with a shoulder and a hole diameter of 20 and 5 mm, respectively. It is worth noting that the selection of FSBE parameters was based on initial investigations with rotational speed of 400−1200 r/min and axial traverse speed of 25−85 mm/min. Since FSBE with a rotational speed of 600 r/min resulted in the extrusion of uniform wire, the wires were fabricated using this rotational speed. Besides, different axial traverse speeds were studied in this work.

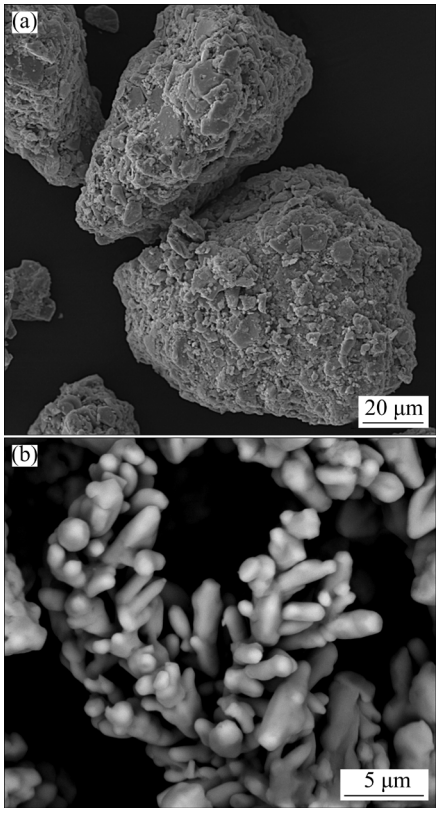

Fig. 1 SEM images of Ti_2SnC powder (a), and copper powders (b)

After extrusion, different samples were prepared to investigate the microstructure, mechanical, wear, and electrical properties. The composite wire

cross-section was prepared using sandpaper and alumina solution to investigate its microstructure. Then, using a mixed solution of 85 mL distilled water, 15 mL HCl, and 5 g $FeCl_3$, the cross-section of the samples was etched to reveal the microstructure. The microstructure was examined using an NGF−120A optical microscope and an SEM (Philips-XL30FSEM) equipped with an EDS detector. Furthermore, the Rigaku Ultima IV X-ray diffraction instrument was used to analyze the different phases. The hardness of the samples was measured using a Koopa Universal (UV1) microhardness tester with a load of 100 g and a time of 15 s. The microhardness test was also employed according to the ASTM E384 standard. Moreover, the tensile test was performed using a SANTAM-STM250 tensile test machine with a crosshead speed of 1 mm/min. The tensile test specimen has a gage length of 25 mm and diameter of 5 mm. Besides, the electrical conductivity test was performed on different samples according to the ASTM B63 standard.

3 Simulation of FSBE process

The advanced mesh-free smoothed particle hydrodynamics (SPH) model was employed to simulate the FSBE process in this work. The elements and fixed grid are not constrained to each other in the SPH technique, allowing the workpiece to maintain a high deformation rate during the simulation. As a result, the FSBE is precisely modeled using ABAQUS in explicit mode. The current study used the cubic spline function as an interpolation kernel function to establish discrete points as physical particles. By translating the finite element method (FEM) nodes of each element (eight-node three-dimensional degree of freedom: C3D8R) to SPH particles (continuum particle elements: PC3D), an equivalent SPH model was created with FEM model. It is worth noting that the particle spacing is the same as the FEM element size. By considering 5 vol.% MAX phase in the copper matrix composite, evenly distributed copper and Ti_2SnC phase particles were used in SPH modeling using a subroutine in the ABAQUS. To ensure compatibility during the FEM-SPH conversion, all FEM elements were made cubic.

The dimension of primary composite, punch and container was considered the same as experimental work (Fig. 2). The rotating punch and container are meshed with thermally coupled 4-node 3D bilinear rigid quadrilateral elements as a Lagrangian rigid body. To precisely control punch movement, all punch movement conditions are assigned with regard to the punch reference point. The convective heat transfer coefficient modeled the natural convection heat loss on the container and punch exterior surfaces. The materials in the process have a self-contact in addition to the FSBE punch/workpiece contact. To account for all contact sites between the workpiece and the punch, a general contact interaction will be used. The Coulomb friction model is used to represent the friction between the punch and the workpiece. Temperature, strain rate, and strain are all factors that influence the material flow stress in the process. Therefore, Johnson−Cook model is utilized to model the flow of copper matrix material as follows, and Ti_2SnC MAX phase is defined as rigid particles in the subroutine:

$$\sigma=(A+B\varepsilon^{n})\left[1+C\ln\left(\frac{\dot{\varepsilon}}{\dot{\varepsilon}_0}\right)\right]\left[1-\left(\frac{T-T_{\mathrm{r}}}{T_{\mathrm{m}}-T_{\mathrm{r}}}\right)^{m}\right] \quad (1)$$

where σ is the yield stress, ε is the equivalent plastic strain, $\dot{\varepsilon}$ is the equivalent plastic strain rate, T is the instantaneous temperature of the process, A is the yield stress under reference conditions, B is the strain hardening, and n, m, $\dot{\varepsilon}_0$ and C are the material parameters. The T_{r} and T_{m} are reference and melting point temperatures, respectively. The parameters related to the properties of the material are listed in Table 1.

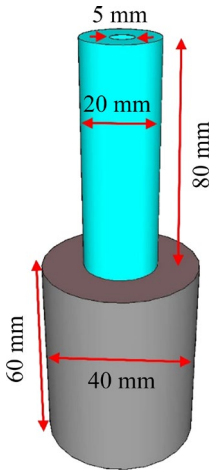

Fig. 2 Dimension of punch and container considered in simulation

Table 1 Johnson−Cook parameters [18,19]

A/MPa	*B*/MPa	*n*	*C*	*m*
90	292	0.31	0.029	0.98

4 Results and discussion

4.1 Microstructure

Figures 3−5 show the optical microscope images of different samples. The average grain size of different samples is shown in Fig. 6. Figures 3(a) and (b) show the microstructures of the unextruded samples before and after sintering, respectively. Moreover, the average grain sizes of unextruded samples before and after sintering are 1.4 and 3.2 μm, respectively. The difference of grain size in the center and near the surface of these samples is not seen.

Figures 4 and 5 show the microstructures of the Cu−Ti_2SnC composite wire fabricated at different extrusion traverse speeds. In addition, Figs. 4(e) and 5(e) show the microstructures of the pure copper wire fabricated at the rotational speed of 600 r/min and traverse speed of 85 mm/min. Under the high-temperature influence and severe plastic deformation during FSBE, grain refinement through dynamic recrystallization happened. Additionally, breaking and improving the distribution of reinforcement particles led to preparing more sites for the nucleation of recrystallized grains [20].

Various factors are influential in determining grain size in FSBEed wires. For example, the plastic strain and temperature are critical in the microstructure of FSBEed wires due to grain refinement induced by the dynamic recrystallization [21,22]. Furthermore, higher plastic strain causes higher dislocation density and more places for nucleation, producing a microstructure with more refined grains. However, it should be noted that a high temperature strongly destroys the effect of applied plastic strain and results in grain growth.

The present study estimated the maximum temperature and plastic strain using a three-dimensional thermo-mechanical model of the FSBE

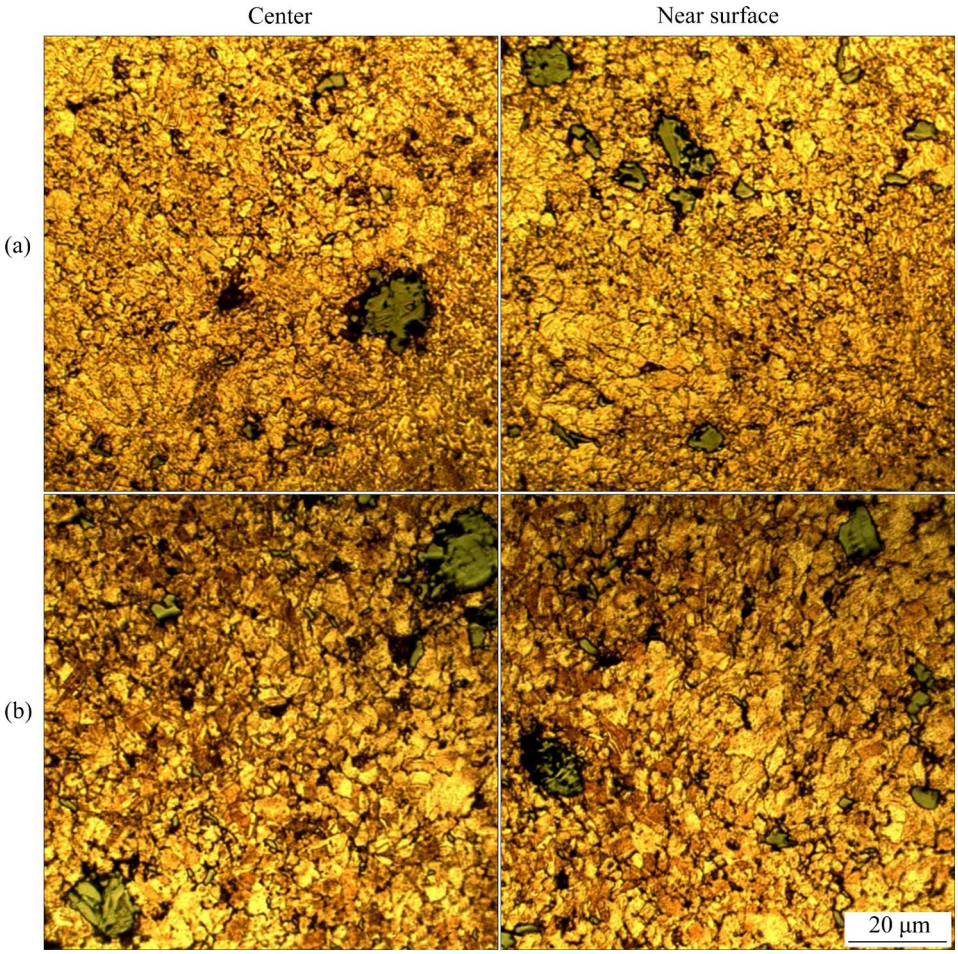

Fig. 3 Optical microscopy images of Cu−Ti_2SnC composite: (a) Before sintering; (b) After sintering

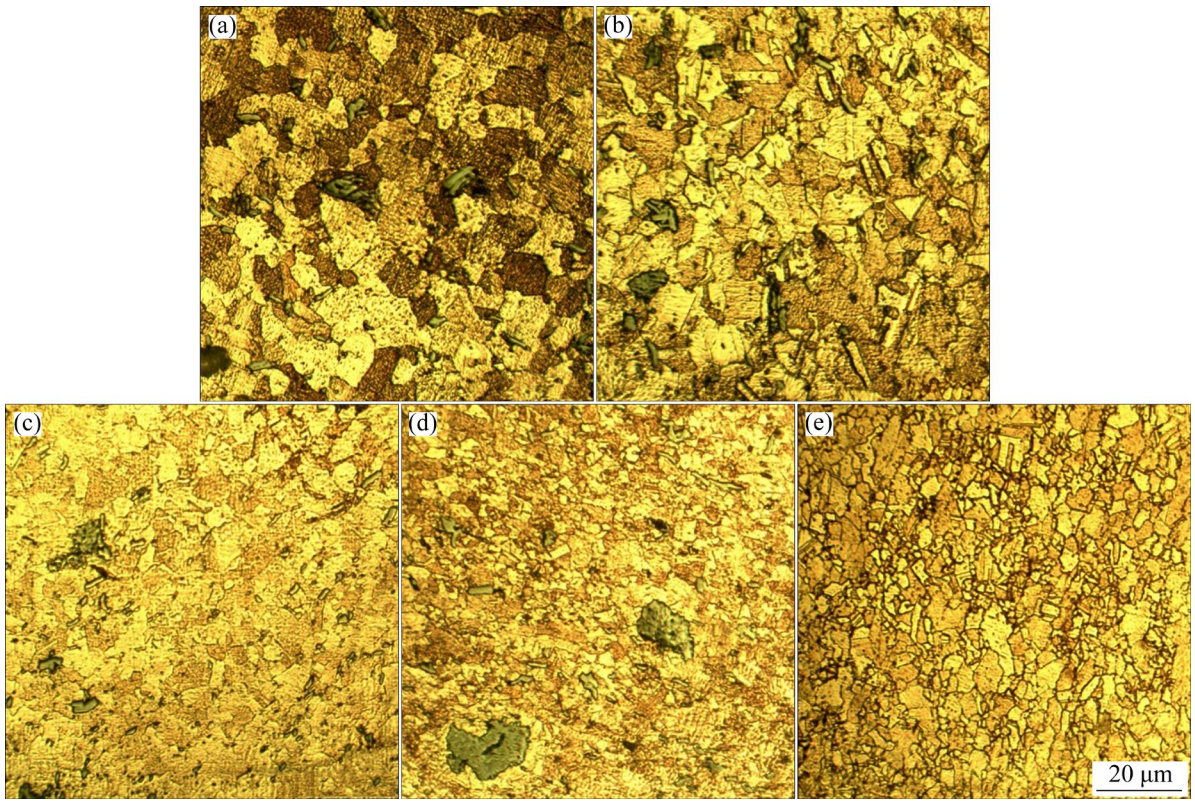

Fig. 4 Optical microscopy images of center zone of Sample 600-25 (a), Sample 600-45 (b), Sample 600-65 (c), Sample 600-85 (d), and Sample 600-85 without reinforcement (e)

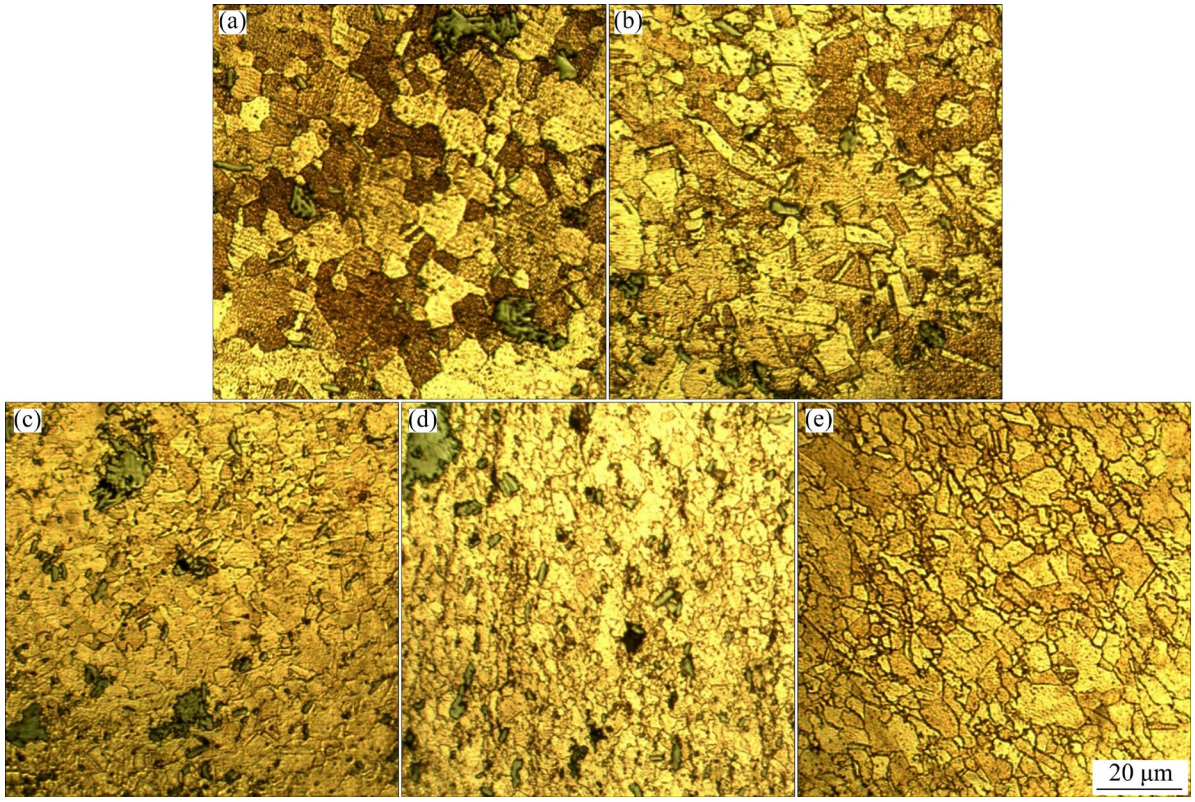

Fig. 5 Optical microscopy images of near surface zone of Sample 600-25 (a), Sample 600-45 (b), Sample 600-65 (c), Sample 600-85 (d), and Sample 600-85 without reinforcement (e)

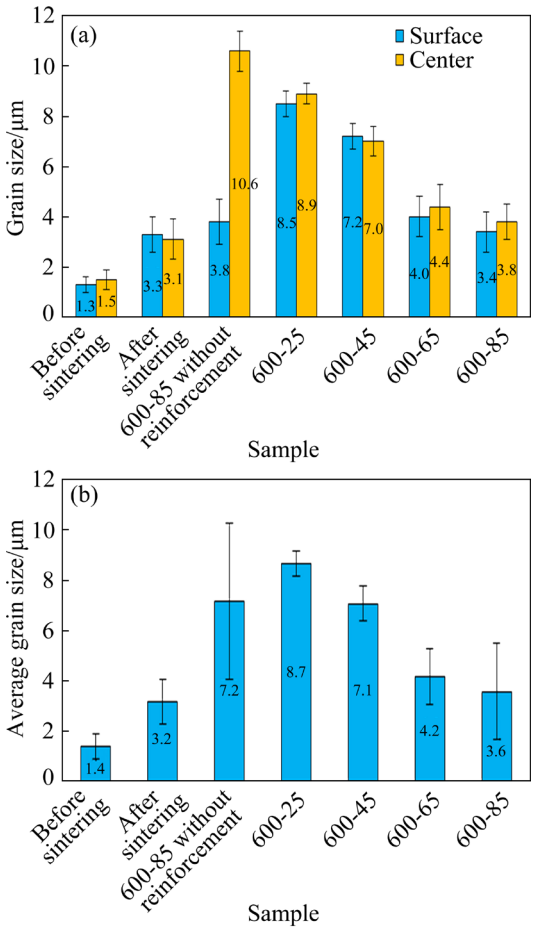

Fig. 6 Grain size distribution at center and near surface of wire (a), and average grain size of different samples (b)

process. It is worth noting that the model was verified using the experimental temperature measurement results. Besides, Table 2 shows that when the extrusion traverse speed increases, the plastic strain and the maximum temperature during FSBE decrease. In this condition, the low temperature does not increase the grain size and the low plastic strain does not decrease the grain size. However, decreasing grain size with increasing the traverse speed shows that the effect of temperature on the grain size reduction is dominant.

Comparing the grain size results of the Sample 600-85 with and without MAX phase particles shows that the absence of MAX phase particles causes the formation of coarser grain size in the extruded sample. The temperature and plastic strain results show that the temperature and plastic strain in the sample without MAX phase particles are higher than those in the sample with them.

The reason for the lower temperature and plastic strain in the sample containing particles may be that the uniform flow ability of the material decreases due to the presence of particles and that the presence of particles through the reduction of the contact surface of copper with the punch and the absorption of a portion of the generated heat by MAX phase causes the sample to have a lower temperature and less plastic deformation. The center and near the surface of wires produced in the FSBE process experienced different strain and temperature levels during the process; thus, the applied strain and temperature were higher near the surface than those in the center [23]. Moreover, the higher plastic strain near the wire surface caused more breaking and more uniform distribution of the reinforcement particles.

Table 2 Maximum temperature and plastic strain of different samples

Sample	Temperature/°C	Plastic strain/%
600-25	843	51.8
600-45	809	42.8
600-65	789	40.1
600-85	764	37.9
600-85 without reinforcement	776	39.6

On the other hand, more strain and finer distribution cause an increment in nucleation locations [16,23]. Consequently, the microstructure near the surfaces should be more refined than that in the center. However, as mentioned, the temperature was higher in this part than that in the center and the grain size increased. But this did not cause a coarse grain size near the surfaces compared to the grain size in the center of the wire. This finding was due to the small broken Ti_2SnC near the surface, acting as an obstacle for further grain growth and causing the grain size near the surface to be almost equal to the grain size in the center. In Figs. 4(e) and 5(e), which are related to pure copper wire, the grain size near the surface is larger than that in the center due to a higher temperature caused by the absence of Ti_2SnC.

The discontinuous interface energy can usually be reduced by metal defects like dislocations, twins, and stacking faults [24]. Moreover, the internal stress causes a lot of dislocations, twin crystals [25], and low strain cause twinning [26]. Besides, reinforcement in grains and grain boundaries prevents the simultaneous formation of annealing

twins and deformation twins [27]. On the other hand, revealing annealing twins in optical microscope images is difficult [28]. As a result, the twins in Figs. 3−5 are the deformation twins [27,28]. In addition, the internal stress applied to composite wires causes twinning. As can be seen in Table 2 and other studies [23], when the extrusion traverse speed increases, the plastic strain decreases and causes more twins at high extrusion speeds.

Figure 7 and Table 3 show the SEM images and energy dispersive spectroscopy (EDS) spot analysis results of different zones of the composite wires and pure copper wire, respectively. Figure 8 shows the EDS results of different points. During the process, under the influence of heat and applied plastic strain, a reactive layer is formed at the interface of the particle and the copper matrix, and the quantity and quality of which vary according to the traverse speed. Although the thickness of the reactive layer is low at traverse speeds of 45, 65, and 85 mm/min, discontinuities are observed at the interface between the MAX phase and the matrix due to the lower flow of copper-induced by less heat and plastic strain. A blue arrow in Fig. 7

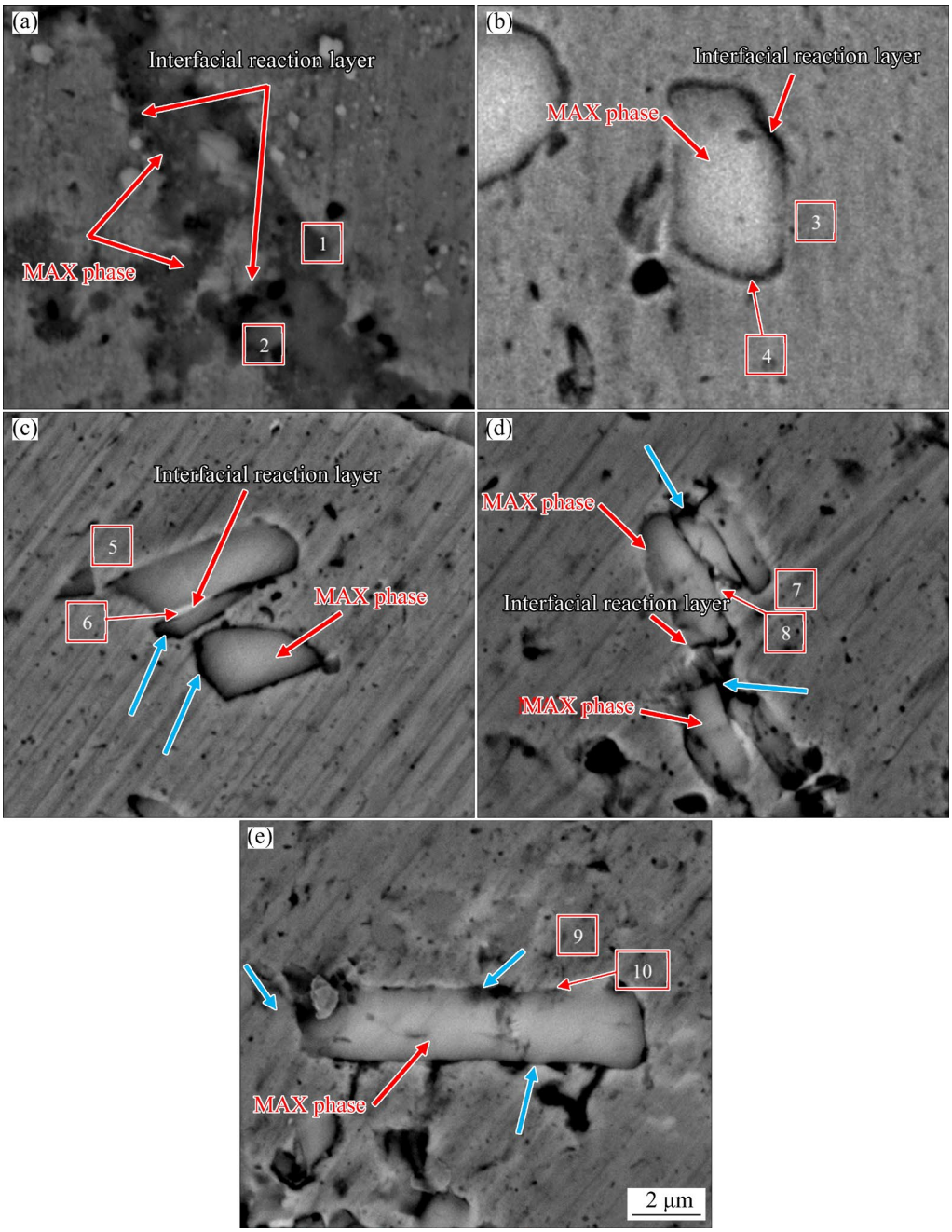

Fig. 7 SEM images of Cu−Ti_2SnC composite after sintering (a), Sample 600-25 (b), Sample 600-45 (c), Sample 600-65 (d), and Sample 600-85 (e)

Table 3 Chemical composition of different points marked in Fig. 7 (at.%)

Element	Spot No.									
	1	2	3	4	5	6	7	8	9	10
Ti	0.10	5.32	0.05	4.96	0.03	4.51	0.15	5.06	0.19	2.70
Sn	0.09	25.12	0.09	13.21	0.04	13.06	0.06	16.30	0.10	15.01
C	0.05	2.86	0.04	1.32	0.02	1.02	0.07	1.55	0.09	1.25
Cu	99.76	66.7	99.82	80.83	99.91	81.41	99.72	77.09	99.62	81.04

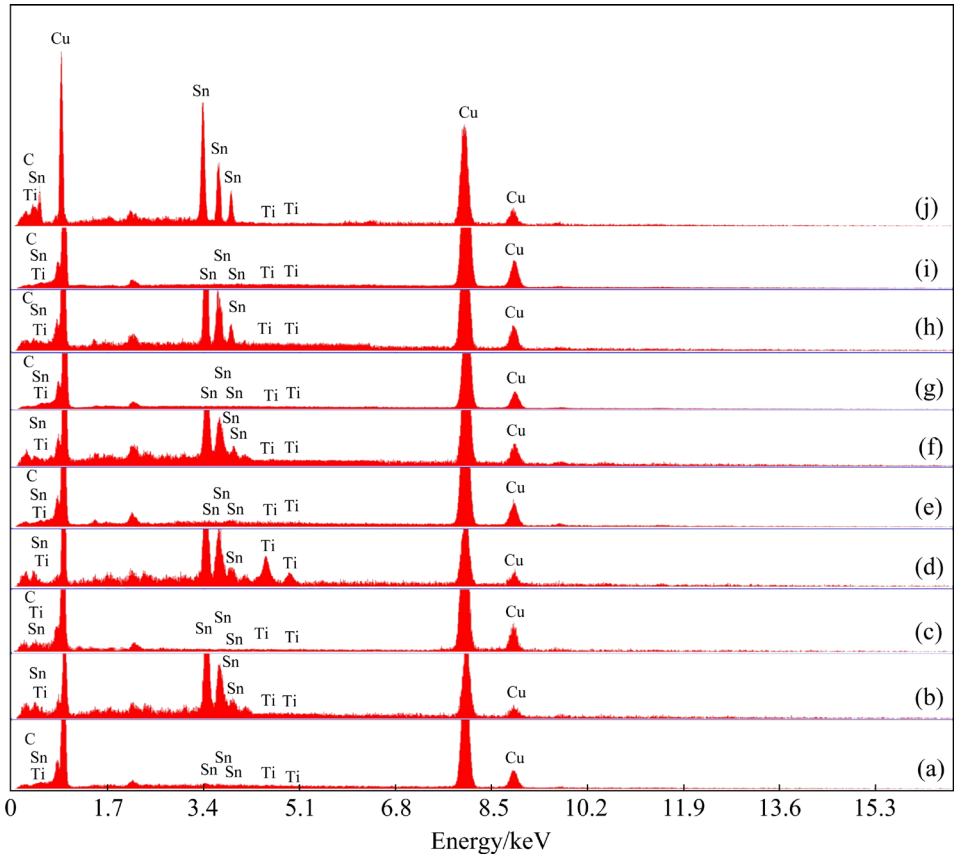

Fig. 8 EDS analysis results of different zones maeked in Fig. 7: (a) Spot 1; (b) Spot 2; (c) Spot 3; (d) Spot 4; (e) Spot 5; (f) Spot 6; (g) Spot 7; (h) Spot 8; (i) Spot 9; (j) Spot 10

represents this discontinuity. Decreasing the traverse speed makes the matrix material flow easier, and a more integrated bond is observed at the interface.

4.2 XRD analysis

The XRD patterns of different samples are presented in Fig. 9. The diffraction patterns of Cu and Ti_2SnC were observed in all samples. Furthermore, by decreasing extrusion traverse speed and generating more heat and plastic deformation, some of the tin in the MAX phase diffused towards the copper matrix, and the $Cu_{81}Sn_{22}$ was formed in the samples. The texture

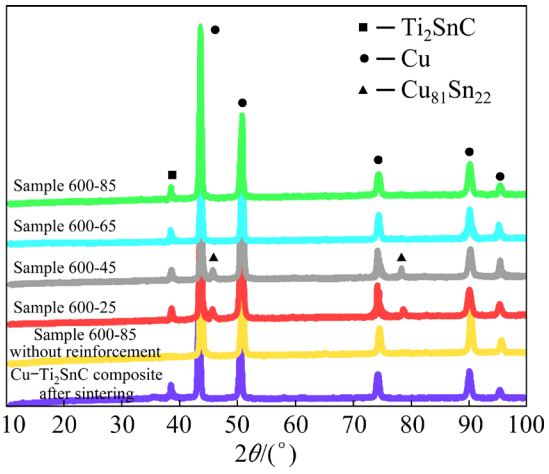

Fig. 9 XRD patterns of different samples

parameter of different samples is shown in Fig. 10. Besides, the texture parameter (TP) was used to calculate grain orientation, according to the following relationship [29]:

$$\mathrm{TP}_{hkl}=\frac{I_{hkl}/R_{hkl}}{\frac{1}{n}\sum_{0}^{n}(I_{hkl}/R_{hkl})} \quad (2)$$

where I_{hkl} is the intensity of {*hkl*} in the primary composite samples and extruded wires, and R_{hkl} is the intensity of {*hkl*} in the same sample with random orientation for *n* peaks. There are three modes for the texture parameter. The TP<1 indicates that these planes are preferentially avoided. TP=1 shows random orientation, and TP>1 represents that {*hkl*} planes are preferentially oriented parallel to the section plane in most grains and also the strength occurred in the (*hkl*) [29]. As can be seen, adding the MAX phase and decreasing the traverse speed caused a significant change in the texture parameter. Moreover, adding the MAX phase to the copper matrix, the {111} and {110} textures were weakened, and the {100} texture was strengthened.

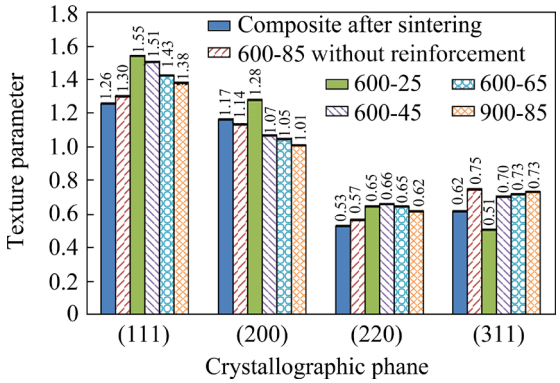

Fig. 10 Texture parameters of different samples

Meanwhile, in the extruded samples, the intensity of the {100} texture was slightly reduced, and the {111} and {110} textures were strengthened compared to the sample before extrusion. It should be noted that the application MAX phase and the extrusion process led to a further increase in the {111} and {110} texture intensity. Based on Ref. [30], strengthening the {111} and {110} textures increased the strength and hardness of copper.

4.3 Mechanical properties

Figure 11 shows the composite wires' micro-hardness profile of Samples 600-25, 600-45, 600-65, and 600-85. In addition, it represents the micro-hardness profile of unreinforced copper wire and primary composite samples before and after sintering. The microhardness distribution in the FSBE processed samples were heterogeneous, probably due to the gradient microstructure creation. The decrease in the hardness of the composite sample after sintering was also probably due to the larger grain size of the copper matrix in the sintered sample and the residual stresses' release in the sample after sintering.

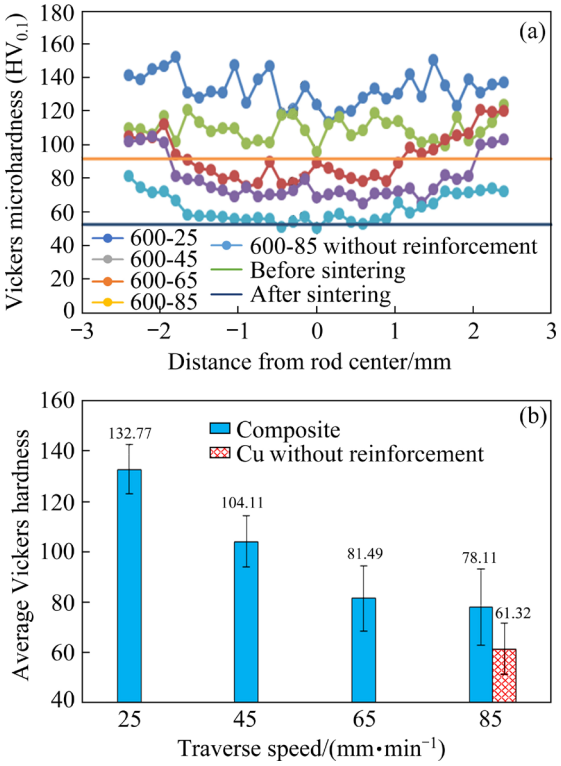

Fig. 11 Vickers microhardness profile (a) and average hardness (b) of different samples

In addition, the FSBE process was performed on the primary composite sample after sintering increased the microhardness. As the extrusion speed increased, the process temperature decreased, and if the process temperature was not high enough to complete sintering, the atoms could not move quickly. In other words, their flowability decreased, and they moved quickly along Ti_2SnC, and atomic diffusion did not occur sufficiently. This poor wettability created an insufficient interfacial bond between the matrix and the reinforcement. Additionally, it caused a large porosity [23,31−34], and Fig. 7 shows the porosity increment trend well.

Although the grain size decreased with increasing extrusion traverse speed, the hardness decreased with increasing extrusion traverse speed. With increasing traverse speed, as shown in Fig. 7, the bond quality at the interface decreased, and porosity formation increased. The presence of non-bonding areas at the MAX−Cu matrix interface could affect the hardness drop in the composite sample. In addition, the finer MAX phase in the samples extruded with lower traverse speed can cause an increasing hardness with decreasing traverse speed. Moreover, the average sizes of MAX phase particles in the Samples 600-25, 600-45, 600-65, and 600-85 were 3.7, 5.2, 6.8, and 7.6 μm, respectively. As can be seen, the hardness of the composite increased by 27% by applying reinforcing particles and carrying out the extrusion process (Sample 600-85) under the influence of the average fixed parameters.

Based on the results of grain size and hardness in the composite sample and the sample without MAX phase, it can be seen that the hardness increases with the increase of grain size. Indeed, the hardness results showed that the strengthening through grain size was not effective in increasing the hardness. Strengthening through the solid solution is one of the strengthening methods in pure metals [35]. Microstructural investigations have shown that the dissolution of MAX particles in the copper matrix increases with decreasing the axial traverse speed. The formation of solid solution at the interface of Cu−Ti_2SnC can affect the strength of the composites through the solid-solution strengthening mechanism. Due to the different thermal expansion coefficients of the reinforcing phase and copper matrix [12,35], thermal mismatch strengthening occurs in the cooling step of the composite. The mismatch of the thermal expansion and modulus of elasticity coefficients between the copper matrix and reinforcement particles creates dislocations in the matrix, which leads to the strengthening of metal matrix composites [36]. The significant difference in the thermal expansion and elastic modulus coefficient of Ti_2SnC reinforcing phase and copper matrix may cause geometrically necessary dislocations (GND). This increase in dislocation density and their interaction causes matrix strengthening. In addition, the load transfer mechanism [37] can also be considered in the Cu−Ti_2SnC composite due to forming a relatively strong bond between the matrix and the reinforcing particles. Although the volume fraction of Ti_2SnC particles is the same in different composite samples, it should be noted that by increasing the axial traverse speed due to the formation of weakness at the interface, it can be expected that the contribution of the load transfer and thermal mismatch strengthening mechanisms is reduced.

The results of the hardness profile in the composite samples also showed almost constant hardness changes, although the hardness was slightly higher at the edges of the wire than that at the center. However, the hardness changes in the central and edge areas of the wire were more in the sample without MAX phase and composite wires processed at higher axial traverse speed (Samples 600-65 and 600-85). On the other hand, noticeable changes in the grain size of these two areas were not observed in the samples, and the distribution of the MAX phase in these areas was almost the same, as reported in other sources [38,39]. However, the plastic strain was more in the edge areas of the wire during the extrusion process compared to the central regions. Furthermore, the dislocation density increases and the residual stress in the edge regions could effectively increase the hardness of the edge regions of wire compared to the central regions of wire. It should be noted that finer grain size at edge of sample without MAX phase can help to this hardness increasing at edge of wire.

Moreover, Fig. 12 shows the tensile test properties of different samples. The yield and ultimate tensile strengths for pure copper wire were 74.32 and 228.76 MPa, respectively. In the composite

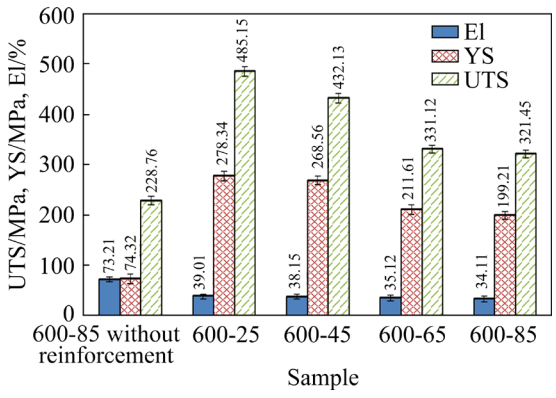

Fig. 12 Tensile test properties of different samples

wire fabricated with similar extrusion parameters (Sample 600-85), the yield strength and ultimate tensile strength reached 199.21 and 321.45 MPa, respectively. The finer grain size and an increase in the {111} and {110} textures intensity compared to the unreinforced sample could be effective in achieving the higher strength in this sample.

In addition, the presence of reinforcement particles limits the movement of dislocations, reduces the plastic deformation, and is a factor for low elongation [40]. The highest elongation (73.21%) was achieved in the pure copper wire, and for its composite wire (Sample 600-85), it was 34.11%. Besides, These values for Samples 600-65, 600-45, and 600-25 reached 35.12%, 38.15%, and 39.01%, respectively, with reducing the traverse speed. These results were due to the improvement of the interface bonding and the reduction of porosities.

The microstructure, constituents, and interfaces determined the mechanical properties of copper matrix composite. It is worth noting that the term large particle is used when the relationship between the matrix and the particle is not discussed at the atomic or molecular level. Moreover, most of the composites of this category consist of a harder reinforcement phase than the matrix [28].

In addition, principal strengthening mechanisms of the CMCs include Hall−Patch strengthening, dislocation strengthening, Orowan strengthening, and thermal expansion mismatch [28]. Besides, the severe plastic deformation at high temperatures during the FSBE process causes grain refinement. This process is executed through dynamic recovery (DRV), geometric dynamic recrystallization (GDRX), and discontinuous dynamic recrystallization (DDRX) due to the low stacking fault energy of copper [28].

On the other hand, applying the FSBE process causes the particles to break and improve their distribution. Additionally, the presence of the reinforcement particles dramatically increases the nucleation sites for recrystallization [41]. This grain size reduction increases the strength of the composite [35]. However, the present study showed that the composite wires did not reduce the grain size compared to the primary composite sample after sintering. Therefore, this mechanism may not have a decisive role in strengthening.

Performing FSBE changes the density of dislocations. Furthermore, the relationship between yield stress and dislocation density for FCC metals is usually expressed by the Taylor's relationship, where the yield stress (σ) is related to the dislocation density (ρ) as follows:

$$\sigma=\sigma_0+M\alpha Gb\rho^{0.5} \tag{3}$$

where σ_0 is the flow stress, α is a constant, M is the average Taylor factor, G is the shear modulus, and b is the amplitude of Burgers vector. They were equal to 20 MPa, 0.5, $\sqrt{3}$, and 41.35 GPa, respectively [35].

As the extrusion speed decreases, the strain increases and causes the density increase of dislocations, but on the other hand, the decrease in extrusion speed increases the temperature. This increment in temperature makes it easier for dislocations to move smoothly and create dislocations without colliding with others in slip systems and causes the dislocation density to decrease [32].

In addition, the thermal expansion mismatch causes geometrically necessary dislocations. Then, this increment in the dislocation density and their interaction cause the copper matrix to be strengthened [35]. However, according to the research on the Cu−5vol.%Ti_2SnC composite, the strength increase due to this mechanism was only a few tens of MPa [15]. The Orowan mechanism is more pronounced in metal matrix composites with a low reinforcing particle ratio.

Furthermore, dislocations can bypass such particles by the Orowan loop. According to this mechanism, the strength increases by reducing the size of particles and distance. This mechanism is effective when a strong interface occurs between the matrix and the reinforcement. The strong bond between the matrix and the reinforcement is vital in improving mechanical properties. Besides, weak wettability between the copper matrix and the reinforcement causes a large volume of porosity [33].

In the Cu−Ti_2SnC composite, the interdiffusion between Cu and Sn caused the formation of an interfacial reaction layer, resulting in a stronger bond between the matrix and the reinforcement. According to the EDS spot analysis in Table 3, some Sn was found in the copper matrix in the primary composite sample after sintering and extruding composite wires. Additionally, combined with the XRD results, interdiffusion between

copper and tin occurred, leading to the formation of $Cu_{81}Sn_{22}$ and Cu(Sn) solid solution.

In addition, according to the XRD pattern, the Cu−Sn intermetallic quantity was more for Samples 600-25 and 600-45. This finding might be due to the more plastic strain and higher temperature in these samples. Besides, a more suitable bonding between the matrix and the reinforcement reduced the porosity. In the FSBE process, by the extrusion speed reduction, the process temperature increased; consequently, the flowability of material increased, and the porosity decreased.

Apart from the above micromechanics mechanisms, the load transfer ($\Delta\sigma_{LT}$) for copper matrix composites was considered, given the continuum mechanics. This consideration was due to the sufficient interface bonding between the matrix and the reinforcement, expressed by

$$\Delta\sigma_{LT}=\sigma_p v_p \quad (4)$$

where v_p is the volume fraction of the reinforcement particles, and σ_p is the bearing stress by the reinforcement due to the application of shear stress at the interface, expressed by

$$\sigma_p=\tau_i(L/r) \quad (5)$$

where τ_i is shear stress at the interface, and L and r are the longest and shortest dimensions of the particle, respectively.

If the reinforcement particles have an equiaxed morphology, then $L/r\approx1$. On the other hand, the shear strength at the good interface bonding between the matrix and the reinforcement can be considered half of the matrix yield strength ($1.2\ \sigma_{ym}$). As a result, the load must be transferred from the matrix to the reinforcement, increasing the strength. The strengthening in this condition can be expressed as follows [35]:

$$\Delta\sigma_{LT}=1.2\sigma_{ym}v_p \quad (6)$$

According to the explanations mentioned previously, the extrusion speed reduction causes a more uniform interface bonding and the possibility of creating less porosity. Improving the interface bond according to Eqs. (4) and (5) increased the amount of shear stress at the interface, $\Delta\sigma_{LT}$, and the composite strength [35]. In this condition, it can be said that,

$$\Delta\sigma_{LT\ sample\ 600\text{-}25}>\Delta\sigma_{LT\ sample\ 600\text{-}45}>\Delta\sigma_{LT\ sample\ 600\text{-}65}>\Delta\sigma_{LT\ sample\ 600\text{-}85} \quad (7)$$

In addition, Fig. 13 shows the SEM images related to the fracture surfaces of different samples. The dimples and microvoids indicate a ductile fracture. Dimples were the result of coalescence of the microscopic holes. The crack started in the micro-voids and discontinuities between the matrix and the reinforcement. Moreover, the crack propagated along with the weak bond without damaging the particles and caused the reinforcement particles to separate from the matrix, indicating a weak bond. However, the break of reinforcement particles indicated that the bond at the interface was strong.

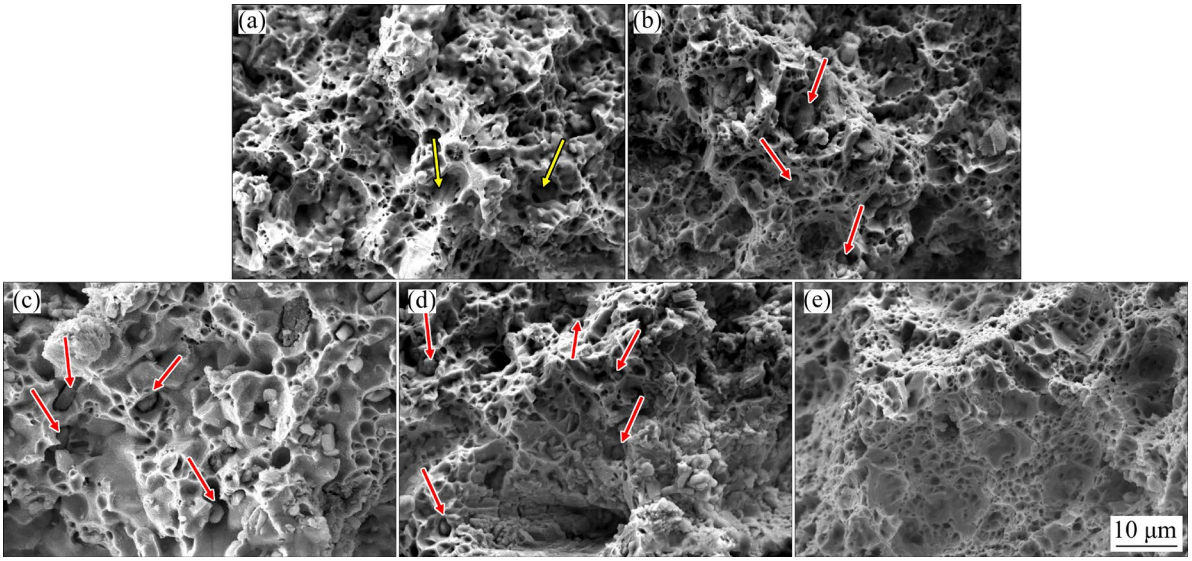

Fig. 13 SEM images of fracture surface of Sample 600-25 (a), Sample 600-45 (b), Sample 600-65 (c), Sample 600-85 (d), and Sample 600-85 without reinforcement (e)

Figures 13(a−d) show the fracture surface of composite samples and Fig. 13(e) shows the fracture surface of pure copper wire. It can be said that with the increase of extrusion speed, the interface bond became weaker, and the porosity increased. Additionally, the crack started from these discontinuities and propagated along with the weak bond. This process caused the separation of the Ti_2SnC particle, the coalescence of this part with the porosity, and the increase of dimple size by the micro-holes.

According to Figs. 13(a) and (b), related to the Samples 600-25 and 600-45, respectively, the dimples' size was smaller due to the more suitable interface bonding. Furthermore, the red arrows indicate the MAX particles reinforcing the fracture surface. As shown in the Samples 600-45, 600-65, and 600-85, the separation between the MAX phase and the copper matrix was evident on the fracture surface. This phenomenon led to weakness at the interface and, consequently, the loss of strength of composite samples. In Sample 600-25, as shown by the yellow arrows, the fracture occurred in the MAX phase particles. This observation confirms the integrity and high quality of the MAX phase−Cu matrix interface.

4.4 Electrical conductivity

The electrical conductivity changes of the extruded samples and the extruded sample without MAX phase are shown in Fig. 14. It can be seen that the electrical conductivity decreased after the composite fabrication. Besides, sample 600-25 showed a higher electrical conductivity than other extruded composite samples. The density of grain boundaries can affect the electrical conductivity, and the electrical conductivity decreases with the grain size reduction in copper [33,42,43]. However, the results showed that the reinforcing particles and the nature of the bond at the interface acted as key factors in determining the electrical conductivity of the extruded Cu−Ti_2SnC composite.

Using the rule of mixtures (ROM), the electrical conductivity of the composite was assumed by Eq. (8), where E_c is the electrical conductivity of composite, E_m is the electrical conductivity of matrix, and E_r is the electrical conductivity of the reinforcement. In addition, V_m and V_r are the volume fractions of the matrix and the reinforcement, respectively.

The electrical conductivity of matrix was equal to the unreinforced copper's electrical conductivity (i.e., 99.84% (IACS)) and the electrical conductivity of Ti_2SnC at 7.83% (IACS) [44]. Thus, the predicted electrical conductivity of Sample 600-85 using ROM was 95.23% (IACS). This value was higher than the electrical conductivity of Sample 600-85 (78.01% (IACS)).

Moreover, the porosity formation at the interface and the smaller grain size in the composite sample can result in lower electrical conductivity than the predicted value. It should also be said that according to the XRD results, the formation of $Cu_{81}Sn_{22}$ reduced the electrical conductivity of the copper matrix composite [14]:

$$E_c=E_mV_m+E_rV_r \quad (8)$$

4.5 Wear resistance

Figure 15 shows the wear rate and friction coefficient of different samples. The wear rate of pure copper wire was 0.0091 mg/m, and its friction coefficient was 0.65. Besides, the reinforcement particles reduce the wear rate of extruded wires.

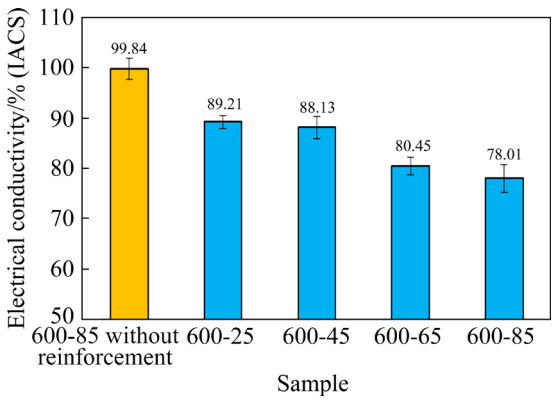

Fig. 14 Electrical conductivity of different samples

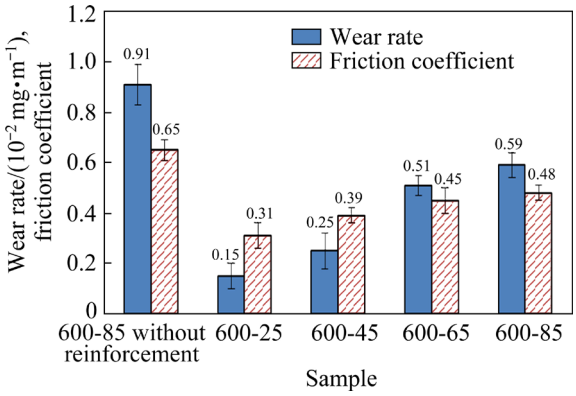

Fig. 15 Wear rate and friction coefficient of different samples

The wear rate reached 0.0059 mg/m for the extruded composite (Sample 600-85). Moreover, the low hardness of pure copper leads to severe material removal and severe plastic deformation on the surface [33]. Adhesive wear is the main reason for the high wear rate of pure copper [10].

In addition, the reinforcement particles act as a barrier between the pin and the matrix and prevent severe removal of the material and adhesive wear [41,45,46]. The wear properties of copper matrix composite are also improved by factors such as uniform distribution of reinforcement, reduction of reinforcement particle size, fine grain microstructure [35], and excellent bonding between the matrix interface and reinforcement. Furthermore, the applied load borne by the particles leads to a decrease in the friction coefficient [28].

On the other hand, the interdiffusion between Cu and Sn causes a strong bond between the matrix and the reinforcement. This bond prevents the separation of Ti_2SnC from the copper matrix and increases the load-bearing capability of Ti_2SnC particles during wear [10]. Additionally, in the softer mated material, there are plowed localized surfaces in the abrasive wear. The plowing of reinforcement particles is due to the poor interface bonding and porosity, and if it happens from plowing to cutting, the mechanism changes to a severe state [47].

With decreasing the traverse speed to 25 mm/min, the friction coefficient and the wear rate decreased and reached the minimum values of 0.31 and 0.0015 mg/m, respectively. According to Refs. [48−50], hardness and wear resistance are directly related, meaning that wear resistance increases as hardness increases. The results of the current study showed that the wear resistance of the composite increased with the increase in the hardness of the copper matrix composite.

Figure 16 shows the SEM images of the worn surfaces. Figures 16(a−d) correspond to Samples 600-25, 600-45, 600-65, and 600-85, respectively. Moreover, Fig. 16(e) corresponds to the pure copper wire sample. By reducing the extrusion traverse speed, despite an increase in the grain size, the wear rate and the width of the wear scars decreased. This finding had two reasons: (1) a better interface bonding between the matrix and the reinforcement, and (2) a finer and more uniform distribution of the reinforcement particles [28].

It is worth noting that the wear mechanism was adhesive for pure copper, and the contribution of the abrasive wear mechanism increased for the composite wires. In addition, increasing the extrusion traverse speed in the composite wire samples resulted in the plowing of the reinforcement particles (shown by red arrows) in a severe state. This finding was due to improper interface bonding and more porosity.

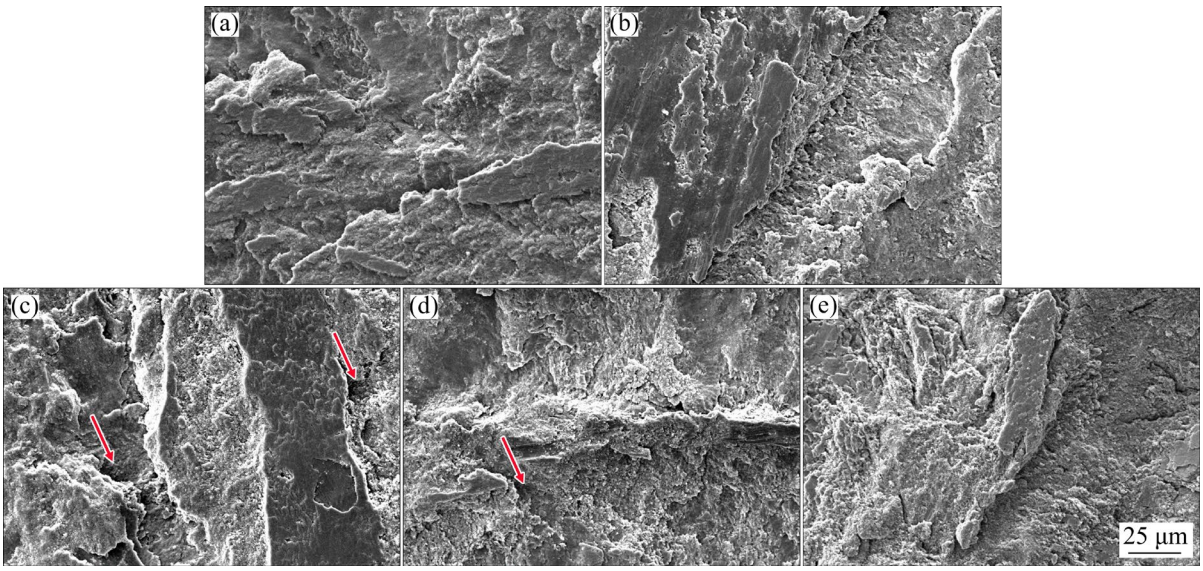

Fig. 16 SEM images of worn surface of Sample 600-25 (a), Sample 600-45 (b), Sample 600-65 (c), Sample 600-85 (d), and Sample 600-85 without reinforcement (e)

5 Conclusions

(1) Reducing the extrusion traverse speed from 85 to 25 mm/min made the Ti_2SnC particles finer, decreased the porosity, and improved the interface bond integrity.

(2) As the extrusion traverse speed increased, the values of twins increased due to the lower strain rate.

(3) Applying MAX phase reinforcing particles and carrying out the extrusion process at a rotational speed of 600 r/min and a traverse speed of 85 mm/min increased the hardness, tensile strength, and wear resistance of the copper matrix to HV 78.11, 321.45 MPa, and 0.0059 mg/m, respectively.

(4) Decreasing the extrusion traverse speed from 85 to 25 mm/min increased the yield strength, ultimate tensile strength, and elongation to 278.34 MPa, 485.15 MPa, and 39.01%, respectively, due to better interfacial bonding and less porosity.

(5) Decreasing the extrusion traverse speed from 85 to 25 mm/min increased the electrical conductivity to 89.21% (IACS) due to the larger grain size, better interface bonding, and lower porosity.

(6) Reducing the extrusion traverse speed from 85 to 25 mm/min decreased the friction coefficient and wear rate by to 0.31 and 0.0015 mg/m, respectively.

CRediT authorship contribution statement

Amirhossein JAHANI: Investigation, Resources, Writing − Original Draft; **Hamed JAMSHIDI AVAL**: Conceptualization, Methodology, Writing − Review & Editing, Supervision; **Mohammad RAJABI:** Conceptualization, Methodology, Writing − Review & Editing, Supervision; **Roohollah JAMAATI:** Conceptualization, Methodology, Writing − Review & Editing, Supervision.

Declaration of competing interest

The authors declare that they have no known competing financial interests or personal relationships that could have appeared to influence the work reported in this paper.

References

[1] SALVO C, CHICARDI E, HERNÁNDEZ-SAZ J, AGUILAR C, GNANAPRAKASAM P, MANGALARAJA R V. Microstructure, electrical and mechanical properties of Ti_2AlN MAX phase reinforced copper matrix composites processed by hot pressing [J]. Materials Characterization, 2021, 171: 110812.

[2] KHALOOBAGHERI M, JANIPOUR B, ASKARI N, SHAFIEE KAMAL ABAD E. Characterisation of powder metallurgy Cu−ZrO_2 composites [J]. Adv Prod Eng Manag, 2013, 8(4): 242−248.

[3] WANG F, LI Y, WANG X, KOIZUMI Y, KENTA Y, CHIBA A. In-situ fabrication and characterization of ultrafine structured Cu−TiC composites with high strength and high conductivity by mechanical milling [J]. Journal of Alloys and Compounds, 2016, 657: 122−132.

[4] DAI S G, LI J W, WANG C J. Preparation and thermal conductivity of tungsten coated diamond/copper composites [J]. Transactions of Nonferrous Metals Society of China, 2022, 32(9): 2979−2992.

[5] WANG J, WANG X W, LI B, CHEN C, LU X F. Interface repairing for AA5083/T2 copper explosive composite plate by friction stir processing [J]. Transactions of Nonferrous Metals Society of China, 2021, 31(9): 2585−2596.

[6] QIN Y Q, TIAN Y, PENG Y Q, LUO L M, ZAN X, XU Q, WU Y C. Research status and development trend of preparation technology of ceramic particle dispersion strengthened copper-matrix composites [J]. Journal of Alloys and Compounds, 2020, 848: 156475.

[7] LUO S W, WU Y, CHEN B, SONG M, YI J H, GUO B S, WANG Q W, YANG Y, LI W, YU Z T. Effects of Cu content on microstructures and compressive mechanical properties of CNTs/Al−Cu composites [J]. Transactions of Nonferrous Metals Society of China, 2022, 32(12): 3860−3872.

[8] JAMWAL A, MITTAL P, AGRAWAL R, GUPTA S, KUMAR D, SADASIVUNI K K, GUPTA P. Towards sustainable copper matrix composites: manufacturing routes with structural, mechanical, electrical and corrosion behaviour [J]. Journal of Composite Materials, 2020, 54(19): 2635−2649.

[9] SINGH M K, GAUTAM R K. Synthesis of copper metal matrix hybrid composites using stir casting technique and its mechanical, optical and electrical behaviours [J]. Transactions of the Indian Institute of Metals, 2017, 70(9): 2415−2428.

[10] WU J Y, ZHOU Y C, WANG J Y. Tribological behavior of Ti_2SnC particulate reinforced copper matrix composites [J]. Materials Science and Engineering: A, 2006, 422(1/2): 266−271.

[11] GAO P, LIU Z X, TIAN B, TONG Y X, CHEN F, LI L. Microstructure, phase transformation and mechanical properties of NiMnGa particles/Cu composites fabricated by SPS [J]. Transactions of Nonferrous Metals Society of China, 2022, 32(10): 3291−3300.

[12] SUN Z M. Progress in research and development on MAX phases: A family of layered ternary compounds [J]. International Materials Reviews, 2011, 56(3): 143−166.

[13] JAHANI A, JAMSHIDI AVAL H, RAJABI M, JAMAATI R. Effects of Ti_2SnC MAX phase reinforcement content on the properties of copper matrix composite produced by friction stir back extrusion process [J]. Materials Chemistry and Physics, 2023, 299: 127497.

[14] WU J Y, ZHOU Y C, WANG J Y, WANG W, YAN C K. Interfacial reaction between Cu and Ti_2SnC during processing of Cu−Ti_2SnC composite [J]. International Journal of Materials Research, 2005, 96(11): 1314−1320.

[15] WU J Y, ZHOU Y C, YAN C K. Mechanical and electrical properties of Ti_2SnC dispersion-strengthened copper [J]. International Journal of Materials Research, 2005, 96(8): 847−852.

[16] WU J Y, CHAI K. Strengthening of Cu−Ti_2SnC composites due to microstructural changes in the material [J]. Key Engineering Materials, 2007, 353: 429−432.

[17] LI X, ZHOU C, OVERMAN N, MA X L, CANFIELD N, KAPPAGANTULA K, SCHROTH J, GRANT G. Copper carbon composite wire with a uniform carbon dispersion made by friction extrusion [J]. Journal of Manufacturing Processes, 2021, 65: 397−406.

[18] MEYERS M A. Dynamic behavior of materials [M]. John Wiley & Sons, 1994.

[19] GRĄZKA M, JANISZEWSKI J. Identification of Johnson−Cook equation constants using finite element method [J]. Engineering Transactions, 2012, 60(3): 215−223.

[20] ZHANG S H, FREDERICK A, WANG Y Y, ELLER M, MCGINN P, HU A M, FENG Z L. Microstructure evolution and mechanical property characterization of 6063 aluminum alloy tubes processed with friction stir back extrusion [J]. JOM, 2019, 71(12): 4436−4444.

[21] ASADI P, AKBARI M. Numerical modeling and experimental investigation of brass wire forming by friction stir back extrusion [J]. The International Journal of Advanced Manufacturing Technology, 2021, 116(9): 3231−3245.

[22] AKBARI M, ASADI P. Optimization of microstructural and mechanical properties of brass wire produced by friction stir extrusion using Taguchi method [J]. Proceedings of the Institution of Mechanical Engineers, Part L: Journal of Materials: Design and Applications, 2021, 235(12): 2709−2719.

[23] AKBARI M, ASADI P. Brass wire forming by friction stir back extrusion: Numerical modeling and experiment [J]. The International Journal of Advanced Manufacturing Technology, 2021, 116: 3231−3245.

[24] YANG K M, MA Y C, ZHANG Z Y, ZHU J, SUN Z B, CHEN J S, ZHAO H H, SONG J, LI Q, CHEN N Q, MA Y H, ZHOU J, LIU Y, FAN T X. Anisotropic thermal conductivity and associated heat transport mechanism in roll-to-roll graphene reinforced copper matrix composites [J]. Acta Materialia, 2020, 197: 342−354.

[25] CELEBI_EFE G, ALTINSOY I, IPEK M, ZEYTIN S, BINDAL C. Some properties of Cu−SiC composites produced by powder metallurgy method [J]. Metallic Materials, 2011, 49(2): 131−136.

[26] HUANG K, LOGÉ R E. A review of dynamic recrystallization phenomena in metallic materials [J]. Materials & Design, 2016, 111: 548−574.

[27] ĎURIŠINOVÁ K, ĎURIŠIN J, OROLÍNOVÁ M, ĎURIŠIN M, SZABÓ J. Effect of mechanical milling on nanocrystalline grain stability and properties of Cu−Al_2O_3 composite prepared by thermo-chemical technique and hot extrusion [J]. Journal of Alloys and Compounds, 2015, 618: 204−209.

[28] DINAHARAN I, SARAVANAKUMAR S, KALAISELVAN K, GOPALAKRISHNAN S. Microstructure and sliding wear characterization of Cu/TiB_2 copper matrix composites fabricated via friction stir processing [J]. Journal of Asian Ceramic Societies, 2017, 5(3): 295−303.

[29] DICKSON M J. The significance of texture parameters in phase analysis by X-ray diffraction [J]. Journal of Applied Crystallography, 1969, 2(4): 176−180.

[30] SHINDE A B, OWHAL A, SHARMA A, RANJAN P, ROY T, BALASUBRAMANIAM R. Comparative analysis of mechanical properties for mono and poly-crystalline copper under nanoindentation–Insights from molecular dynamics simulations [J]. Materials Chemistry and Physics, 2022, 277: 125559.

[31] TAHMASBI K, MAHMOODI M, TAVAKOLI H. Corrosion resistance of aluminum alloy AA7022 wire fabricated by friction stir extrusion [J]. Transactions of Nonferrous Metals Society of China, 2019, 29(8): 1601−1609.

[32] TAHMASBI K, MAHMOODI M. Evaluation of microstructure and mechanical properties of aluminum AA7022 produced by friction stir extrusion [J]. Journal of Manufacturing Processes, 2018, 32: 151−159.

[33] BARMOUZ M, GIVI M K B. Fabrication of in situ Cu/SiC composites using multi-pass friction stir processing: Evaluation of microstructural, porosity, mechanical and electrical behavior [J]. Composites Part A: Applied Science and Manufacturing, 2011, 42(10): 1445−1453.

[34] CHU K, JIA C C. Enhanced strength in bulk graphene–copper composites [J]. Physica Status Solidi (a), 2014, 211(1): 184−190.

[35] BAHADOR A, UMEDA J, HAMZAH E, YUSOF F, LI X, KONDOH K. Synergistic strengthening mechanisms of copper matrix composites with TiO_2 nanoparticles [J]. Materials Science and Engineering: A, 2020, 772: 138797.

[36] CHENG C, SONG K X, MI X J, WU B A, XIAO Z, XIE H F, ZHOU Y J, GUO X H, LIU H T, CHEN D B, SHEN X Y, DING Y. Microstructural evolution and properties of Cu−20wt.%Ag alloy wire by multi-pass continuous drawing [J]. Nanotechnology Reviews, 2020, 9(1): 1359−1367.

[37] TONG W Z, FANG D, BAO C X, TAN S L, LIU Y C, LI F X, YOU X, TAO J M, BAO R, LI C J, YI J H. Enhancing mechanical properties of copper matrix composite by adding SiO_2 quantum dots reinforcement [J]. Vacuum, 2022, 195: 110682.

[38] ABDI BEHNAGH R, SAMANTA A, AGHA MOHAMMAD POUR M, ESMAILZADEH P, DING H T. Predicting microstructure evolution for friction stir extrusion using a cellular automaton method [J]. Modelling and Simulation in Materials Science and Engineering, 2019, 27(3): 035006.

[39] ZHANG H, LI X, DENG X, REYNOLDS A P, SUTTON M A. Numerical simulation of friction extrusion process [J]. Journal of Materials Processing Technology, 2018, 253: 17−26.

[40] BARMOUZ M, ASADI P, GIVI M K, TAHERISHARGH M. Investigation of mechanical properties of Cu/SiC composite fabricated by FSP: Effect of SiC particles' size and volume fraction [J]. Materials Science and Engineering: A, 2011, 528(3): 1740−1749.

[41] SABBAGHIAN M, SHAMANIAN M, AKRAMIFARD H R,

ESMAILZADEH M. Effect of friction stir processing on the microstructure and mechanical properties of Cu−TiC composite [J]. Ceramics International, 2014, 40(8): 12969−12976.

[42] ABBAS S F, SEO S J, PARK K T, KIM B S, KIM T S. Effect of grain size on the electrical conductivity of copper–iron alloys [J]. Journal of Alloys and Compounds, 2017, 720: 8−16.

[43] TAKATA N, LEE S H, TSUJI N. Ultrafine grained copper alloy sheets having both high strength and high electric conductivity [J]. Materials Letters, 2009, 63(21): 1757−1760.

[44] DING J X, TIAN W B, ZHANG P G, ZHANG M, CHEN J, ZHANG Y M, SUN Z M. Preparation and arc erosion properties of Ag/Ti_2SnC composites under electric arc discharging [J]. Journal of Advanced Ceramics, 2019, 8(1): 90−101.

[45] GAO Y B, LI X Y, MA Y J, KITCHEN M, DING Y T, LUO Q S. Formation mechanism and wear behavior of gradient nanostructured Inconel 625 alloy [J]. Transactions of Nonferrous Metals Society of China, 2022, 32(6): 1910−1925.

[46] CALDATTO DALAN F, DE LIMA ANDREANI G F, TRAVESSA D N, FAIZOV I A, FAIZOVA S, CARDOSO K R. Effect of ECAP processing on distribution of second phase particles, hardness and electrical conductivity of Cu−0.81Cr−0.07Zr alloy [J]. Transactions of Nonferrous Metals Society of China, 2022, 32(1): 217−232.

[47] UMALE T, SINGH A, REDDY Y, KHATITRKAR R K, SAPATE S G. Abrasive wear behaviour of COPPER-SiC and COPPER-SiO_2 composites [J]. International Journal of Modern Physics: Conference Series, 2013, 22: 416−423.

[48] FATHY A, SHEHATA F, ABDELHAMEED M, ELMAHDY M. Compressive and wear resistance of nanometric alumina reinforced copper matrix composites [J]. Materials & Design, 2012, 36: 100−107.

[49] TJONG S C, LAU K C. Abrasive wear behavior of TiB_2 particle-reinforced copper matrix composites [J]. Materials Science and Engineering: A, 2000, 282(1/2): 183−186.

[50] LI M Y, CHAO M J, LIANG E J, YU J M, ZHANG J J, LI D C. Improving wear resistance of pure copper by laser surface modification [J]. Applied surface science, 2011, 258(4): 1599−1604.

挤压速度对搅拌摩擦反挤压法制备 Cu−5%Ti_2SnC 复合丝材性能的影响

Amirhossein JAHANI, Hamed JAMSHIDI AVAL, Mohammad RAJABI, Roohollah JAMAATI

Department of Materials Engineering, Babol Noshirvani University of Technology, Shariati Avenue, Babol, 47148-71167 Iran

摘　要：对粉末冶金法制备的含 5% (体积分数) Ti_2SnC MAX 相的初始复合材料进行搅拌摩擦反挤压(FSBE)处理，研究 FSBE 工艺的轴向横移速度对 Cu−Ti_2SnC 复合线材显微组织、力学性能、电学性能和磨损性能的影响。结果表明，随着挤压速度的增加，显微组织中孪晶增多，Ti_2SnC 颗粒细化，MAX 相和 Cu 基体之间的界面结合改善。当转速为 600 r/min，轴向横移速度为 25 mm/min 时，Cu−Ti_2SnC 复合线材具有最大的硬度、屈服强度和极限抗拉强度，分别为 HV 132.7、278.34 MPa 和 485.15 MPa，这是其更强的界面结合和更细的 MAX 相导致的。此外，当转速为 600 r/min，轴向横移速度为 25 mm/min 时，Cu−Ti_2SnC 复合丝的电导率最高，达到 89.21% (IACS)，磨损率最低，为 0.0015 mg/m，这是其更大的晶粒尺寸、更强的界面结合与更低的密度导致的。

关键词：搅拌摩擦反挤压；Ti_2SnC MAX 相；铜基复合材料；电导率

(Edited by Xiang-qun LI)